Supplementary data for:

Sequence-dependent nanometer-scale conformational dynamics of individual RecBCD-DNA complexes

Ashley R. Carter[1], Maasa H. Seaberg[2,3], Hsiu-Fang Fan[4, 6], Gang Sun [5], Christopher J. Wilds[5], Hung-Wen Li[6], and Thomas T. Perkins[3,7,*]

[1] Department of Physics, Amherst College, Amherst, Massachusetts, 01002, USA

[2] Department of Physics, University of Colorado, Boulder, Colorado, 80309, USA

[3] JILA, National Institute of Standards and Technology and University of Colorado, Boulder, Colorado, 80309, USA

[4] Department of Life Sciences and Institute of Genome Sciences, National Yang-Ming University, Taipei, 11221, Taiwan

[5] Department of Chemistry and Biochemistry, Concordia University, Montreal, Quebec, H4B1R6, Canada

[6] Department of Chemistry, National Taiwan University, Taipei, 10617, Taiwan

[7] Department of Molecular, Cellular, and Developmental Biology, University of Colorado, Boulder, Colorado, 80309, USA

*To whom correspondence should be addressed. Tel: 1-303-492-5291; Fax: 1-303-492-5235; Email: tperkins@jila.colorado.edu

Present Address: Maasa H. Seaberg, Mayo Clinic, Rochester, Minnesota, 55905, USA

Supplementary Data

Supplementary Methods

DNA constructs. We prepared the DNA (Supplementary Figure S1) using polymerase chain reaction (PCR; GeneAmp XL PCR Kit, Applied Biosystems) from the M13mp18 plasmid (Bayou Biolabs, Genbank accession number X02513). In assays where we bound the DNA directly to the surface and to the bead, we made the DNA construct [(L= 2,979 bp (1,007 nm)] using one biotin-labelled primer and one digoxigenin-labelled primer. For unwinding assays, we prepared a blunt-ended DNA construct [L = 7,249 bp (2,413 nm)] by performing PCR with a biotin-labelled forward primer and an unlabelled reverse primer. There is one chi-site on this DNA template located 5,942 bp from the biotin label; however, the low ATP concentration (2 μM) used in the assay suppresses chi-site recognition (1). In assays where we bound RecBCD to a blunt-ended DNA molecule, we used a similar procedure except the forward primer started at base 3,310 and the reverse primer ended at base 6,248 creating a molecule with a length of 2,939 bp (993 nm). This sequence was selected because it contains a BsmBI restriction site and a DrdI restriction site, which was used to create the tailed DNA constructs.

Tailed DNA constructs with a biotin label at the opposite end were created by cutting the 2,939-bp, blunt-ended DNA molecule with a BsmBI restriction endonuclease (New England Biolabs) so that the purified product had a length of 2,667 bp (901 nm). We then purchased a series of DNA oligonucleotides (Integrated DNA Technologies) to ligate to the cut end. One oligonucleotide had a 5′ sequence complementary to the BsmBI overhang and a 3′-$(dT)_6$ tail. The other oligonucleotide had a 3′ complementary sequence to the first oligonucleotide and a 5′-$(dT)_x$ tail where x = 6, 8, 10, or 20. For GC-rich or AT-rich substrates, the oligonucleotides were designed such that the five base-pairs adjacent to the ssDNA-dsDNA junction were either GC or AT, respectively. Complementary oligonucleotides were annealed at 70 ˚C, slowly cooled (4 ˚C increments held for 30 s) to room temperature, and ligated using T4 DNA ligase (Invitrogen, 16 ˚C for 16 hours, 50:1 molar ratio of annealed oligonucleotide to long DNA). We gel purified the product and concentrations were determined by UV absorption. The final length of the tailed DNA substrates was 2,686 bp (908 nm). To verify the final product, we performed a restriction digest using DrdI (New England BioLabs) on a portion of the final product. This digestion produced a 2,452-bp DNA molecule containing the biotin label, and a 234-bp DNA molecule with the tailed substrate. If the BsmBI digestion were faulty, a band would appear at 487 bp for the blunt-ended DNA molecule and, if the ligation was fault, there would be a band at 215 bp for the DNA molecule with the BsmBI cut end.

The tailed DNA construct with the interstrand crosslink was prepared using a slightly different procedure. To ligate the cross-linked tails to the 2,667-bp DNA cut with BsmBI, we had to add two other oligonucleotides to the ligase reaction. These two oligonucleotides (5′-/5Phos/CTGGTCTGGTCTGGT-3′ and 5′-/5Phos/GTGCCACCAGACCAGA-3′) contain the 5′-CTGG-3′ sequence that is complementary to the BsmBI overhang and the 5′-GTGCC-3′ sequence that is complementary to the overhang in the cross-linked oligonucleotide construct. After the ligase reaction, the DNA construct was 2,694 bp (911 nm).

As a control, we also prepared a tailed DNA construct that could bind directly to the coverslip. Oligonucleotides in this case were purchased with either a biotin or digoxigenin label. Control measurements of DNA length at 6 pN showed that this DNA construct exhibited a noise level that was indistinguishable from DNA without the 5′-$(dT)_{10}$ tail (Supplementary Figure S5). All DNA

constructs were gel purified and the resulting final concentrations quantified using a spectrophotometer (Genova, Jenway).

Cross-linked oligonucleotide preparation and purification. 5′-*O*-Dimethoxytrityldeoxyribonucleoside-3′-*O*-(β-cyanoethyl-*N*,*N*'-diisopropyl) phosphoramidites and protected deoxyribonucleoside polystyrene (PS) supports (50 nm) were purchased from Glen Research. 3′-*O*-Dimethoxytrityldeoxyribonucleoside-5′-*O*-(β-cyanoethyl-*N*,*N*′-diisopropyl) phosphoramidites were purchased from ChemGenes, Inc. The fully protected cross-linked phosphoramidite was prepared with slight modifications to published procedures (2). The cross-linked duplexes were assembled on a 1-μmol scale using a synthesizer (Model 3400, Applied Biosystems) employing standard b-cyanoethylphosphoramidite chemistry supplied by the manufacturer with slight modifications to coupling times. The nucleoside phosphoramidites containing standard protecting groups were dissolved in anhydrous acetonitrile to a concentration of 0.1 M for the 3′-*O*-deoxyphosphoramidites, 0.15 M for the cross-linked 3′-*O*-deoxyphosphoramidite, and 0.2 M for the 5′-*O*-deoxyphosphoramidites. Assembly of sequences was carried out in four steps: (*i*) detritylation: 3% trichloroacetic acid in dichloromethane; (*ii*) nucleoside phosphoramidite coupling time of 2 min for commercial 3′-*O*-deoxyphosphoramidites, 3 min for 5′-*O*-deoxyphosphoramidites and 10 min for the cross-linked phosphoramidite; (*iii*) capping: acetic anhydride/pyridine/tetrahydrofuran 1:1:8 (v/v/v) and 1-methylimidazole/tetrahydrofuran 16:84 (w/v); and (*iv*) oxidation: 0.02 M iodine in tetrahydrofuran/water/pyridine 2.5:2:1. The terminal trityl group was removed by the synthesizer.

The oligonucleotide-derivatized supports were transferred from the reaction column to screw-cap microcentrifuge tubes fitted with teflon-lined caps. The protecting groups were removed by treatment with a 3:1 mixture of concentrated ammonium hydroxide and ethanol for 4 h at 55 ºC. The cross-linked duplexes were purified by strong anion exchange high-performance liquid-chromatographic (SAX HPLC) columns using a DNAPAC PA-100 column (0.4 cm × 25 cm) purchased from Dionex Corp. in a linear gradient of 20–55% buffer B (0.1 M Tris HCl, pH 7.5, 1 M NaCl, 10% acetonitrile) over 30 min at 40 ºC. The columns were monitored at 260 nm for analytical runs or 280 nm for preparative runs. The purified oligonucleotides were desalted using C-18 SEP PAK cartridges (Waters Corp.) as previously described (3).

The composition of the cross-linked oligonucleotides (0.1 A_{260} units) were confirmed enzymatically using a combination of snake venom phosphodiesterase (0.28 units) and calf intestinal phosphatase (5 units) in a buffer containing 10 mM Tris (pH 8.1) and 2 mM magnesium chloride for 16 h at 37 °C as previously described (3). The resulting mixture of nucleosides was analyzed by reversed phase HPLC carried out using a Symmetry C-18 5-μm column (0.46 cm × 15 cm) purchased from Waters Corp. The C-18 column was eluted with a linear gradient of 0–60% buffer (50 mM sodium phosphate, pH 5.8, 50% acetonitrile) over 30 min. The resulting peaks were identified by co-injection with the corresponding standards. The masses of the oligonucleotides were determined by electrospray ionization (ESI) mass spectrometry and were in agreement with the expected values.

Flow chamber assembly. Samples were constructed by first fabricating fiducial marks onto the coverslip and then building a flow cell from the coverslip and a slide. We fabricated hydrogen-silesquinone (HSQ, FOx-16, Dow Corning) or silicon fiducial marks onto KOH-cleaned cover slips for use in active stabilization (4,5). To enhance usability in single-molecule assays, the cover slips were cleaned with a 10-min piranha dip (100 mL sulfuric acid and 15 drops hydrogen

peroxide at 80 ˚C) after nanofabrication. We constructed epoxy-rigidified flow chambers (internal volume ~15 μL) for enhanced stability using double-sided tape (3M) as a spacer and 5-min epoxy (ITW Devcon) for rigidity. Cover slips were recovered (>20 times) and cleaned after use by soaking the flow chamber in boiling water for 1 h (to remove the cover slip) and piranha cleaning the cover slip for 10 min. Surface chemistry after such cleaning was compatible with single-molecule force spectroscopy experiments.

Tethered bead assay. To determine the unwinding activity of RecBCD, we prepared the samples as stated and placed them on the microscope. We then counted the number of bead-DNA complexes, often referred to as tethers, that were attached to the surface over a ~50 × 50 μm^2 area, only including those tethers that exhibited tethered Brownian motion consistent with the correct DNA length. We added 10 μM ATP to the sample, which allowed RecBCD to unwind the DNA over a period of several minutes. Visual inspection of enzymatic motion showed that the tethered bead motion decreased and, hence, DNA length decreased. RecBCD complexes were labeled as active if either the RecBCD unwound the DNA such that there was almost no bead motion at ~20 mins later, or RecBCD ran off the end of the DNA after unwinding and the bead diffused away. Activity was calculated as the ratio of the number of active tethers to the total number of tethers.

Precision optical-trapping microscope. Our highly stable optical-trapping system was based on earlier work (6). Briefly, out setup consisted of a high-powered, trapping laser (Millennia IR, 10 W, λ = 1064 nm, Spectra-Physics,) and two detection lasers (VPSL, 50 mW, λ = 785 nm and 850 nm, Blue Sky Research) for measuring bead motion and stage drift. In the image plane (Fig. 1*A*), the two diode lasers were positioned so as to scatter light off either a fiducial mark or an optically trapped bead. Both the forward-scattered light and the incident beams were collected by the condenser and were imaged onto a quadrant photodiode (QPD, YAG-444-4A, PerkinElmer Optoelectronics) to detect position (7-9). Bead position (x_{bd}) was used to calculate DNA contour length (L) (10) and thereby infer RecBCD translocation. Fiducial mark position (x_{fid}, y_{fid}, z_{fid}) was used in a feedback loop to a 3D, closed-loop, piezoeletric (PZT) stage (P517.3CD, Physik Instrumente) to keep sample position constant. Position of the fiducial mark or trapped bead was detected by a QPD (250 kHz bandwidth with custom electronics; ~40 μW laser power at detector). Lateral motion was deduced from the normalized intensity difference on the QPD while vertical motion was deduced by the sum signal, the total light falling upon the four quadrants of the QPD. The normalized differences, as well as the offset-amplified sum signal, were digitized using 16 bits at either 4 or 10 kHz using appropriately set antialiasing filters (Frequency Devices).

Data collection and analysis.

To measure the motion of the enzyme along the DNA, we first determined the vertical location of the surface by monitoring the sum signal as a tethered bead was brought into contact with the surface. We calibrated the trapped bead position and then lowered the stage 300 nm. We found the lateral tether point position by performing a 2D elasticity-centering procedure, which also returned the persistence length. We stretched the DNA along the y-axis to a force of 6 pN (unless otherwise specified) by moving the PZT stage. A corresponding move of the fiducial-tracking laser was necessary to keep the fiducial mark centered. After recalibrating the fiducial mark, we actively stabilized the sample using a software-based feedback loop with a 100-Hz update rate and a proportional gain of 0.05. Concurrent with measuring fiducial mark position, the software

(LabVIEW 8.5) also measured the trapped bead position to determine DNA length (10). We note that our DNA length (L) is actually the length from the bead to the surface anchor point as shown in Figure 2E. Thus, changes in L could be from changes in DNA length or from conformational dynamics within RecBCD. The collected raw data at 4 or 10 kHz was smoothed with a moving fourth order Savitzky-Golay or binomial window to the specified frequency, typically either 1, 5, or 10 Hz.

For measuring RecBCD movement, we implemented either a force clamp or a pseudo force clamp in parallel with the above stage stabilization. RecBCD-driven unwinding of the DNA causes motion of the bead relative to the trap center, which changes the force. In the pseudo force clamp, we keep the force within 15% of the initial value by allowing the trapped bead to move ±10 nm from the clamp position (70 nm). Bead displacement outside of this range was brought back to 70 nm via stage motion, with a corresponding displacement of the laser that tracks the fiducial mark. In the force clamp, the bead position was maintained at the 70 nm using a stage-based feedback loop that updated every 10 ms.

To detect steps within the data, we fit the data using a step-finding algorithm based on a maximum likelihood parameter (11). The step finding algorithm assumed the data was either increasing or decreasing, and required a user defined input for the number of steps in the data. The number of steps was determined by plotting the maximum likelihood parameter vs. number of steps, and choosing a value to the left of the peak, as described previously (11). Data at 100 Hz was smoothed to 5 or 10 Hz with a fourth order Savitzky-Golay window before being input into the step finding program.

To determine the level of conformational dynamics in the data, we calculated a mean standard deviation. We did this by selecting a 30-s section of the positional trace and calculating the power spectral density of the raw data at 10 kHz using a Hanning window and a segment length of 2^{17} points. For the case where RecBCD was unwinding the DNA in the presence of ATP, we used 100 Hz data and a segment length of 2^{11} points. Then, we integrated the power spectral density over the band 0.1–10 Hz to compute the standard deviation, and averaged the individual standard deviations from multiple traces to obtain the mean standard deviation ($\bar{\sigma}$). The mean standard deviations for all conditions are listed in Supplementary Table S1.

Simulated RecBCD Motion. To simulate high-resolution records of RecBCD, we first concatenated a 30 s trace of RecBCD stalled in the middle of the DNA without any ATP (Figure 2A, *Stalled*) 150 times to create a trace that was 4,286-s long since the total recorded time for all high-resolution records of RecBCD is 4,286 s. This 100-Hz trace was smoothed to 5 Hz with a Savitzky-Golay filter. Second, we simulated a trace with either 1 bp or 4 bp exponentially distributed steps (Supplementary Figure S3). The kinetic rate for the steps (0.3 nm/s) matched the analyzed portion of the high-resolution records of RecBCD motion. Finally, we added our simulated stepping trace to the concatenated trace of RecBCD stalled in the middle of the DNA without ATP.

To analyze the simulated data, we used a step finding algorithm (11) to determine the number and size of the steps in the trace. We then histogrammed the steps sizes output by the algorithm and fit the forward step sizes with a Gaussian distribution, extracting the mean and width of the distribution. For the simulated data containing 1-bp and 4-bp steps, there was a broad range (±100) in the number of steps that were found by the step finding algorithm. We chose a round value in the middle of this range as the number of steps found (1,000 steps for the simulated data with 1-bp steps and 1,600 steps for the simulated data with 4-bp steps). We then fit the histogram of the

1-bp stepping record to a Gaussian, yielding a peak of 5.5 ± 2.8 bp (mean ± width) (Supplementary Figure S3). If instead we input the actual number of steps into the step finding algorithm (4,000), the peak of the Gaussian was unaltered (5.4 ± 3.3 bp). Likewise, the simulated data containing the 4-bp steps had a histogram with a Gaussian peak and width of 5.5 ± 2.3 bp for the 1,600 found steps or 5.7 ± 2.4 bp using the actual number of steps.

Supplementary Figures

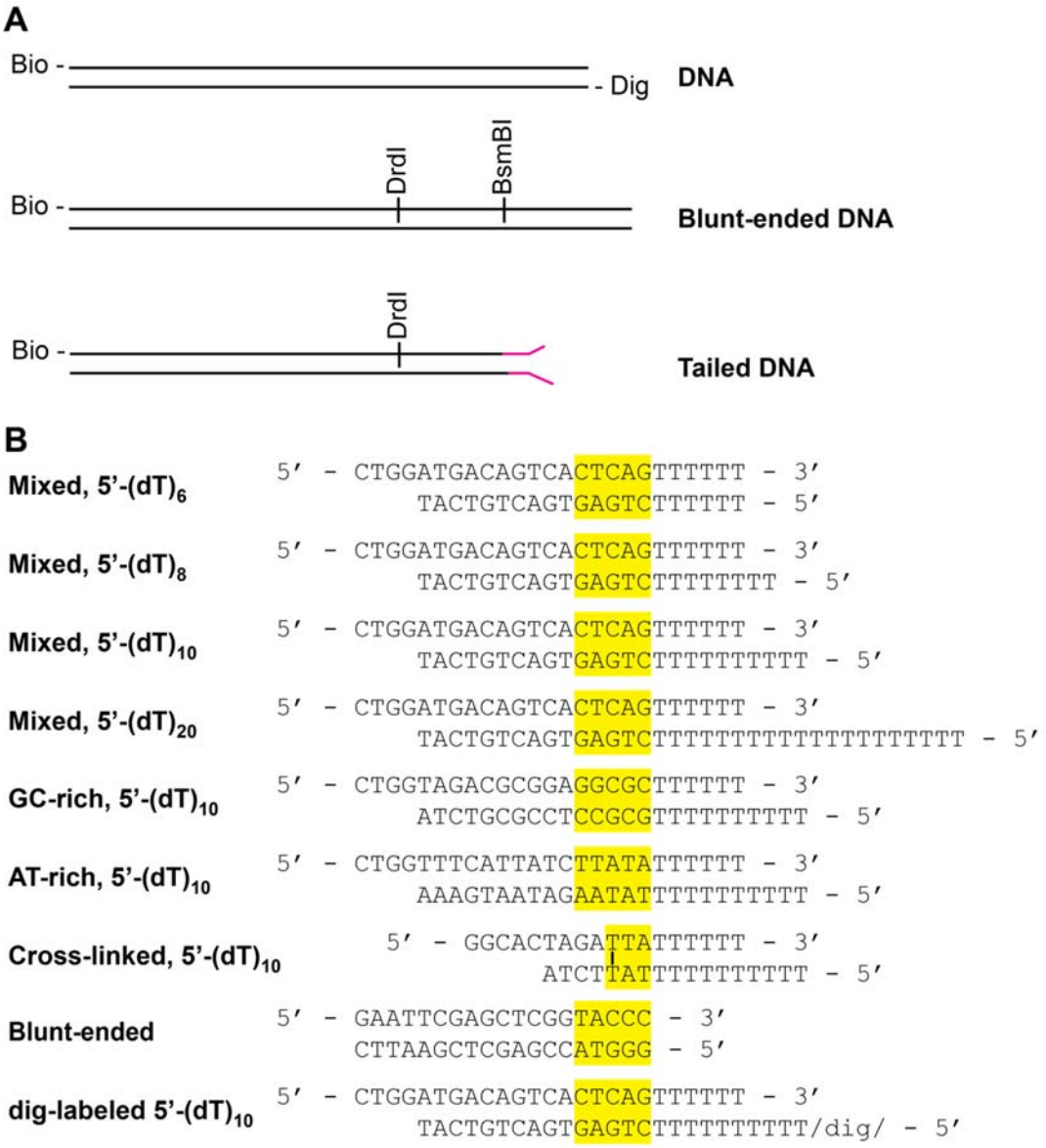

Supplementary Figure S1. DNA constructs. (**A**) Overview of the DNA constructs used to create our single molecule assay. The biotin (Bio) and digoxigenin (Dig) tags, along with the restriction sites, are marked. Tailed ends are shown colored (*pink*). (**B**) Sequences of the DNA constructs showing the upstream duplex DNA and the poly T tails, if present. The five basepairs immediately ahead of the ssDNA-dsDNA junction—two in the case of the cross-linked substrate—is highlighted (yellow).

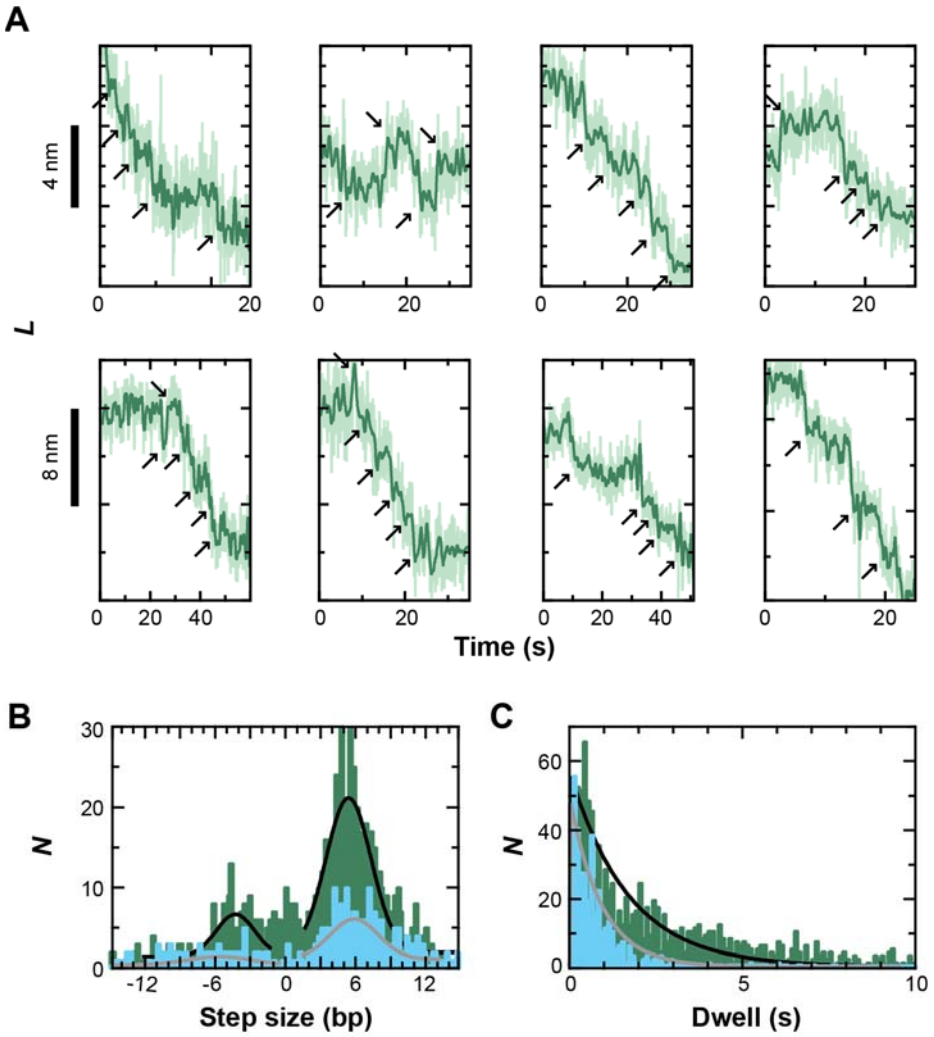

Supplementary Figure S2. Discrete translocations exhibited by RecBCD during active unwinding at low ATP are variably sized in both the forward and backward direction. (**A**) Traces of deduced contour length *L* show forward motion of RecBCD against 6 pN with 2-μM ATP. The records were smoothed to 10 Hz (*light green*) and 1 Hz (*dark green*). Discrete translocations were determined using a step-fitting algorithm (*black arrows*). (**B**) Histogram of the determined step sizes for all of the 2-μM-ATP (*green*) and 4-μM-ATP (*light blue*) data show variably sized forward and backward motion. Gaussian fits (*black* and *gray*, respectively) to the histogram reveal a peak at 5.3 ± 2.3 bp (mean ± σ) for forward motion and 4.6 ± 2.2 bp for backward motion at 2 μM ATP. At 4 μM ATP, analysis yield 5.4 ± 2.3 bp for forward motion and 5.5 ± 3.6 bp for backward motion. (**C**) Histogram of the dwell times for each step is fit to a gamma function. At both ATP concentrations, the fitted parameter *n* is 1.0 ± 0.1, consistent with 1-rate-limited step. Color coding is the same as in **B**.

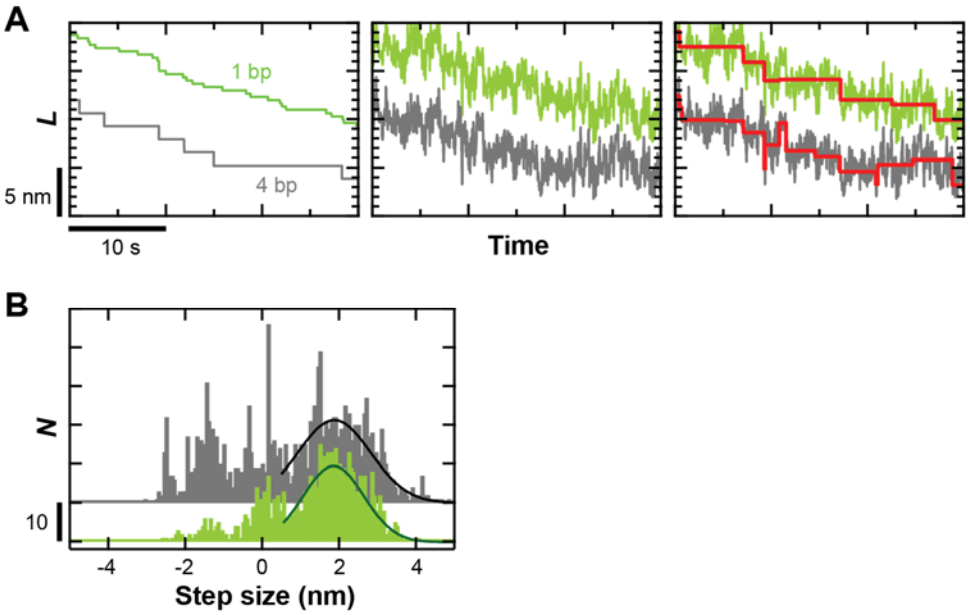

Supplementary Figure S3. Simulations show that step-size determination was dominated by RecBCD's conformational dynamics. (**A**) *Left panel*: A portion of two traces with simulated steps of either 1 bp (*green*) or 4 bp (*gray*) with an average velocity of 0.3 nm/s. *Middle panel*: Similar traces with added conformational dynamics based on the experimentally measured dynamics of a stalled RecBCD in the middle of the DNA (Figure 2A, *Stalled*) smoothed to 5 Hz. *Right panel:* Data in the middle panel replotted with the steps (*red*) found by a widely used step finding algorithm (11). (**B**) Histograms of the fitted step sizes for the trace with the simulated 1-bp (*green*) and 4-bp (*gray*) steps were fit by to a Gaussian, yielding a peak and width of 5.5 ± 2.8 bp and 5.5± 2.3 bp, respectively. The 4-bp step-size histogram was vertically offset for clarity

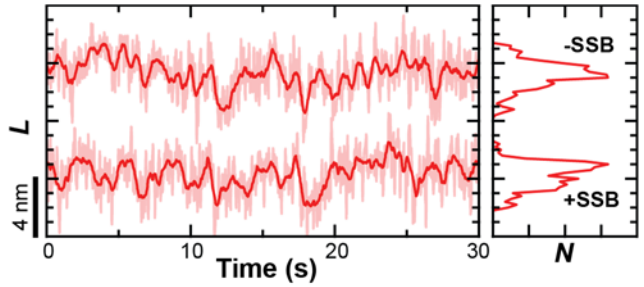

Supplementary Figure S4. Conformational dynamics are not dependent on SSB. Measurement of *L* for RecBCD stalled on partially unwound DNA due to removal of ATP (*red*) shows similar behavior in the absence of SSB (-*SSB*) and in the presence of SSB (+*SSB*). Traces smoothed to 10 Hz (*light*) and 1 Hz (*dark*). Histograms are of the 1 Hz traces.

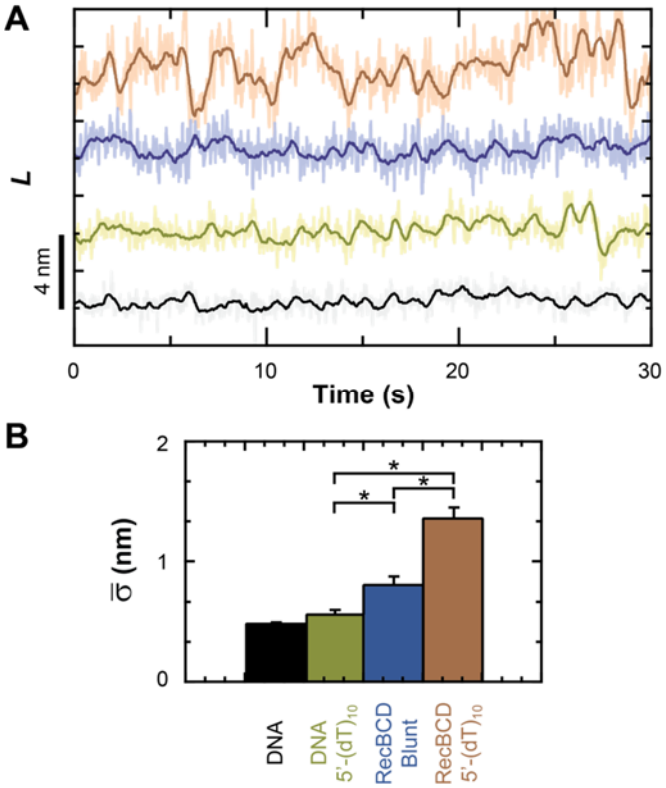

Supplementary Figure S5. DNA with a T-tailed construct bound to the surface is indistinguishable from blunt-ended DNA bound directly to the surface. (**A**) Measurement of *L* for the following conditions in the absence of ATP: RecBCD bound to DNA with a 3′-$(dT)_6$ and 5′-$(dT)_{10}$ tail (*brown*), RecBCD bound to blunt-ended DNA (*blue*), DNA with a 3′-$(dT)_6$ and 5′-$(dT)_{10}$ tail attached directly to the surface (*olive*), and DNA with a blunt-ended attached to the surface (*black*). Traces smoothed to 10 Hz (*light*) and 1 Hz (*dark*). (**B**) Bar graph of the mean standard deviation for the conditions in **A**.

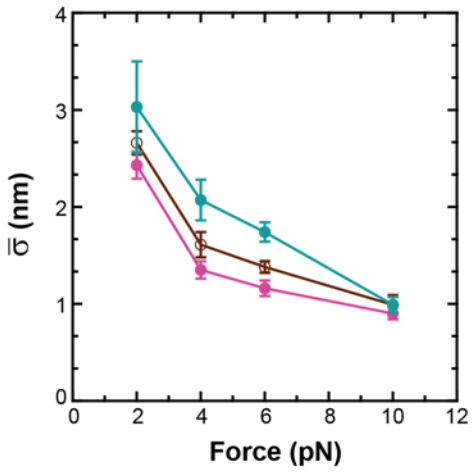

Supplementary Figure S6. Conformational dynamics are dependent on force. Mean values of the integrated fluctuations for RecBCD bound to 5′-$(dT)_{10}$ tailed DNA ends with either the first five upstream base-pairs as A-T (*teal*), mixed sequence (*brown*), or G-C (*pink*) at different forces ($N \geq 5$). Lines between points are included to guide the eye. Error bars denote standard error of the mean.

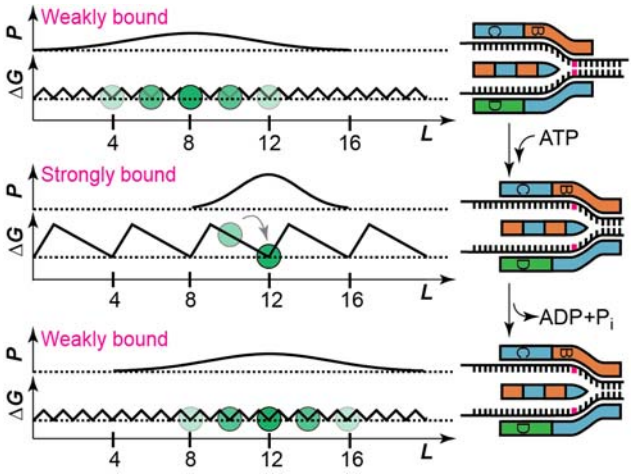

Supplementary Figure S7. Conceptual diagram for a flashing ratchet model of helicase unwinding. In such a simplistic toy model, unwinding is generated by alternating between a weakly bound and strongly bound state. In the absence of ATP, the helicase is weakly bound to the DNA and the free energy change (ΔG), to move one base pair along a DNA molecule of length L is relatively small. In this state, diffusion allows the helicase to move back and forth along the DNA, and the probability (P) for the helicase to be at a particular position on the DNA is low. Upon ATP binding, such diffusive motion is suppressed by a change in the free energy landscape. The new free energy profile favors a particular position on the DNA, creating a high probability that the helicase will be found at that position. The alternation between these two states along with an asymmetric free energy landscape in the weakly bound state can drive forward motion, as observed in model physical systems (12).

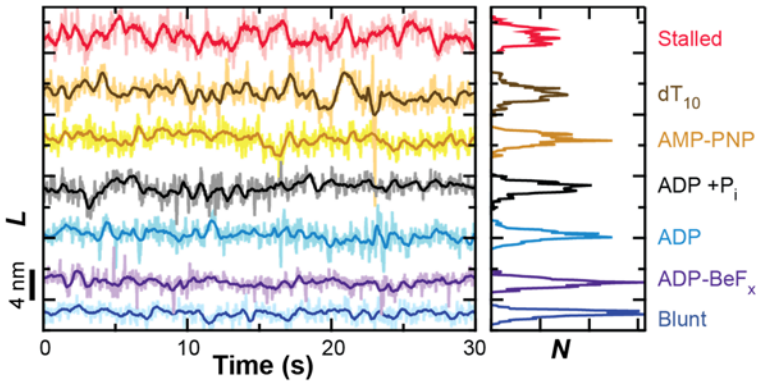

Supplementary Figure S8. Effect of ATP analogues on RecBCD's conformational dynamics. Measurements of *L* for RecBCD bound to the tailed DNA construct with 5′-$(dT)_{10}$ and 3′-$(dT)_6$ ssDNA tails in the following buffer conditions: no ATP (*brown*), 2 mM AMP-PNP (*yellow*), 2 mM ADP + P_i (*gray*), 2 mM ADP (*light blue*), 2 mM ADP-BeF_x (*purple*). For comparison, we show RecBCD bound to blunt-ended DNA (*dark blue*) and RecBCD stalled in the middle of the DNA (*red*). Data is smoothed to 10 Hz (*lighter shades*) and 1 Hz (*darker shades*). Histograms are of the 1 Hz traces.

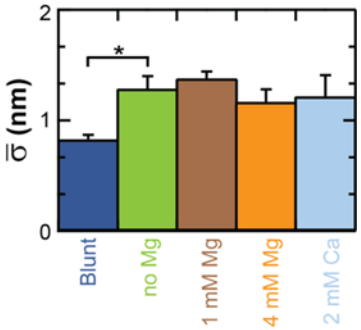

Supplementary Figure S9. Effect of divalent cations on RecBCD's conformational dynamics. Bar graph of the mean standard deviation for RecBCD bound to 5′-$(dT)_{10}$ DNA in the following buffer conditions: no Mg (*green*), 1 mM $Mg(C_2H_3O_2)_2$ (*brown*), 4 mM $Mg(C_2H_3O_2)_2$ (*orange*), and 2 mM $CaCl_2$ (*light blue*). Also shown is RecBCD bound to blunt-ended DNA (*blue*) in 1 mM $Mg(C_2H_3O_2)_2$.

Supplementary Tables

1	DNA	14	0.53 ± 0.02
2	RecBCD, unwinding DNA, ATP	5	1.42 ± 0.12
3	RecBCD, stalled on partially unwound DNA	6	1.42 ± 0.09
4	RecBCD, blunt-ended DNA	8	0.87 ± 0.05
5	RecBCD, 3'-$(dT)_6$ and 5'-$(dT)_6$ tails and mixed upstream sequence	5	0.84 ± 0.05
6	RecBCD, 3'-$(dT)_6$ and 5'-$(dT)_8$ tails and mixed upstream sequence	5	0.98 ± 0.12
7	RecBCD, 3'-$(dT)_6$ and 5'-$(dT)_{10}$ tails and mixed upstream sequence	28	1.38 ± 0.06
8	RecBCD, 3'-$(dT)_6$ and 5'-$(dT)_{20}$ tails and mixed upstream sequence	12	1.39 ± 0.12
9	RecBCD, 3'-$(dT)_6$ and 5'-$(dT)_{10}$ tails and AT-rich upstream sequence	14	1.74 ± 0.10
10	RecBCD, 3'-$(dT)_6$ and 5'-$(dT)_{10}$ tails and GC-rich upstream sequence	10	1.16 ± 0.08
11	RecBCD, 3'-$(dT)_6$ and 5'-$(dT)_{10}$ tails and an intrastrand xlink	7	0.96 ± 0.02
12	RecBCD, 3'-$(dT)_6$ and 5'-$(dT)_{10}$ tails and mixed upstream sequence, ADP	5	1.24 ± 0.14
13	RecBCD, 3'-$(dT)_6$ and 5'-$(dT)_{10}$ tails and mixed upstream sequence, ADP + P_i	5	1.22 ± 0.07
14	RecBCD, 3'-$(dT)_6$ and 5'-$(dT)_{10}$ tails and mixed upstream sequence, ADP-BeF_x	8	0.92 ± 0.05
15	RecBCD, 3'-(dT)6 and 5'-(dT)10 tails and mixed upstream sequence, AMP-PNP	4	1.22 ± 0.19
16	5'-$(dT)_{10}$ tailed DNA	5	0.57 ± 0.03
17	RecBCD, 3'-$(dT)_6$ and 5'-$(dT)_{10}$ tails and AT-rich upstream sequence, 2 pN	6	3.03 ± 0.47
18	RecBCD, 3'-$(dT)_6$ and 5'-$(dT)_{10}$ tails and mixed upstream sequence, 2 pN	7	2.66 ± 0.12
19	RecBCD, 3'-$(dT)_6$ and 5'-$(dT)_{10}$ tails and GC-rich upstream sequence, 2 pN	6	2.43 ± 0.14
20	RecBCD, 3'-$(dT)_6$ and 5'-$(dT)_{10}$ tails and AT-rich upstream sequence, 4 pN	6	2.07 ± 0.21
21	RecBCD, 3'-$(dT)_6$ and 5'-$(dT)_{10}$ tails and mixed upstream sequence, 4 pN	6	1.61 ± 0.13
22	RecBCD, 3'-$(dT)_6$ and 5'-$(dT)_{10}$ tails and GC-rich upstream sequence, 4 pN	6	1.35 ± 0.09
23	RecBCD, 3'-$(dT)_6$ and 5'-$(dT)_{10}$ tails and AT-rich upstream sequence, 10 pN	6	0.99 ± 0.08
24	RecBCD, 3'-$(dT)_6$ and 5'-$(dT)_{10}$ tails and mixed upstream sequence, 10 pN	5	0.99 ± 0.10
25	RecBCD, 3'-$(dT)_6$ and 5'-$(dT)_{10}$ tails and GC-rich upstream sequence, 10 pN	6	0.90 ± 0.06

Supplementary Table S1. List of all conditions tested and the associated number of traces and mean standard deviation ± standard error in the mean (SEM) for each condition.

Supplementary References

1. Dohoney, K.M. and Gelles, J. (2001) Chi-sequence recognition and DNA translocation by single RecBCD helicase/nuclease molecules. *Nature*, **409**, 370-374.
2. Wilds, C.J., Noronha, A.M., Robidoux, S. and Miller, P.S. (2004) Mispair-aligned N3T-alkyl-N3T interstrand cross-linked DNA: synthesis and characterization of duplexes with interstrand cross-links of variable lengths. *J Am Chem Soc*, **126**, 9257-9265.
3. Noll, D.M., Noronha, A.M. and Miller, P.S. (2001) Synthesis and characterization of DNA duplexes containing an N(4)C-ethyl-N(4)C interstrand cross-link. *J Am Chem Soc*, **123**, 3405-3411.
4. Carter, A.R., King, G.M. and Perkins, T.T. (2007) Back-scattered detection provides atomic-scale localization precision, stability, and registration in 3D. *Opt. Express*, **15**, 13434-13445.
5. Carter, A.R., King, G.M., Ulrich, T.A., Halsey, W., Alchenberger, D. and Perkins, T.T. (2007) Stabilization of an optical microscope to 0.1 nm in three dimensions. *Appl. Opt.*, **46**, 421-427.
6. Carter, A.R., Seol, Y. and Perkins, T.T. (2009) Precision surface-coupled optical-trapping assays with 1 base-pair resolution. *Biophys. J.*, **96**, 2926-2934.
7. Pralle, A., Prummer, M., Florin, E.-L., Stelzer, E.H.K. and Horber, J.K.H. (1999) Three-dimensional high-resolution particle tracking for optical tweezers by forward scattered light. *Microsc. Res. Tech.*, **44**, 378-386.
8. Gittes, F. and Schmidt, C.F. (1998) Interference model for back-focal-plane displacement detection in optical tweezers. *Opt. Lett.*, **23**, 7-9.
9. Visscher, K., Gross, S.P. and Block, S.M. (1996) Construction of multiple-beam optical traps with nanometer-resolution position sensing. *IEEE J. Sel. Top. Quant. Electron.*, **2**, 1066-1076.
10. Wang, M.D., Yin, H., Landick, R., Gelles, J. and Block, S.M. (1997) Stretching DNA with optical tweezers. *Biophys. J.*, **72**, 1335-1346.
11. Kerssemakers, J.W., Munteanu, E.L., Laan, L., Noetzel, T.L., Janson, M.E. and Dogterom, M. (2006) Assembly dynamics of microtubules at molecular resolution. *Nature*, **442**, 709-712.
12. Faucheux, L.P., Bourdieu, L.S., Kaplan, P.D. and Libchaber, A.J. (1995) Optical thermal ratchet. *Phys Rev Lett*, **74**, 1504-1507.